HHS Public Access

Author manuscript

J Chem Inf Model. Author manuscript; available in PMC 2016 November 18.

Published in final edited form as:

J Chem Inf Model. 2016 June 27; 56(6): 1184–1192. doi:10.1021/acs.jcim.6b00115.

Synergistic Allosteric Mechanism of FBP and Serine for Pyruvate Kinase M2 *via* Dynamics Fluctuation Network Analysis

Jingxu Yang[#1], **Hao Liu**[#1], **Xiaorui Liu**[#2,3], **Chengbo Gu**[1], **Ray Luo**[4,*], and **Hai-Feng Chen**[1,5,*]

[1]State Key Laboratory of Microbial metabolism, Department of Bioinformatics and Biostatistics, College of Life Sciences and Biotechnology, Shanghai Jiaotong University, 800 Dongchuan Road, Shanghai, 200240, China

[2]International Peace Maternity and Child Health Hospital, School of Medicine, Shanghai Jiao Tong University, Shanghai 200030, China.

[3]Institute of Embryo-Fetal Original Adult Disease Affiliated to Shanghai Jiao Tong University School of Medicine, Shanghai 200030, China.

[4]Departments of Molecular Biology and Biochemistry, Chemical Engineering and Materials Science, Biomedical Engineering, University of California, Irvine, California 92697-3900, USA

[5]Shanghai Center for Bioinformation Technology, 1278 Keyuan Road, Shanghai, 200235, China

[#] These authors contributed equally to this work.

Abstract

Pyruvate kinase M2 (PKM2) plays a key role in tumor metabolism and regulates the rate-limiting final step of glycolysis. In tumor cells, there are two allosteric effectors of fructose-1,6-bisphosphate (FBP) and serine for PKM2. However, the relationship between FBP and serine for allosteric regulation of PKM2 is unknown. Here we constructed residue/residue fluctuation correlation network based on all-atom molecular dynamics simulations to reveal the regulation mechanism. The results suggest that the correlation network in bound PKM2 is distinctly different from that in the free state, FBP/PKM2, or Ser/PKM2. The community network analysis indicates that the information can freely transfer from the allosteric sites of FBP and serine to the substrate site in bound PKM2, while there exists a bottleneck for information transfer in the network of the free state. Furthermore, the binding free energy between the substrate and PKM2 for bound PKM2

[*]Corresponding authors haifengchen@sjtu.edu.cn; rluo@uci.edu, Tel: 86-21-34204348, Fax: 86-21-34204348.

The authors declare that there is no conflict of interest.

Associated Content

Supporting Information

Figure S1 plots Cα RMSD for all systems. Figure S2 shows interaction between allosteric effector and PKM2.Figure S3 plots correlation network for FBP/PKM2 and Ser/PKM2 systems. Figure S4 shows correlation network for mutant systems. Figure S5 shows two communication pathways between the allosteric site and the substrate site. Figure S6 shows DCCM for FBP/PKM2 and Ser/PKM2. Table S1 lists the relevant residues belonging to each community for free PKM2. Table S2 lists the relevant residues belonging to each community for bound PKM2. Table S3 lists the relevant residues belonging to each community for FBP/PKM2. Table S4 lists the relevant residues belonging to each community for Ser/PKM2. Table S5 lists the relevant residues belonging to each community for FBP modification. Table S6 lists the relevant residues belonging to each community for serine modification. Table S7 lists the relevant residues belonging to each community for FBP and serine modifications. Table S8 lists the relevant residues belonging to each community for S437Y mutant. Table S9 lists the relevant residues belonging to each community for H464A mutant. This material is available free of charge via the Internet at http://pubs.acs.org.

is significantly lower than either of FBP/PKM2 or Ser/PKM2. Thus, a hypothesis of “synergistic allosteric mechanism” is proposed for the allosteric regulation of FBP and serine. This hypothesis was further confirmed by the perturbational and mutational analyses of community networks and binding free energies. Finally, two possible synergistic allosteric pathways of FBP-K433-T459-R461-A109-V71-R73-MG2-OXL and Ser-I47-C49-R73-MG2-OXL were identified based on the shortest path algorithm and were confirmed by the network perturbation analysis. Interestingly, no similar pathways could be found in the free state. The process targeting on the allosteric pathways can better regulate the glycolysis of PKM2 and significantly inhibit the progression of tumor.

Graphical abstract

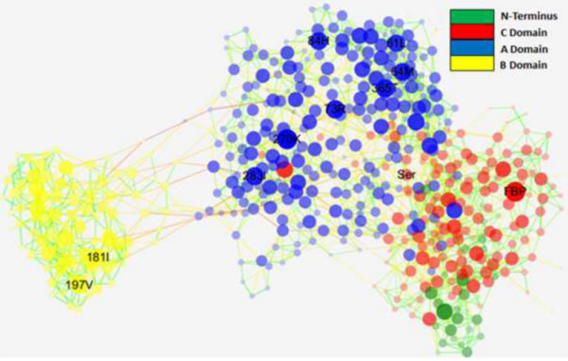

Keywords

PKM2; synergistic allostery; dynamics correlation network; community; allosteric pathway

Introduction

It has been pointed out that metabolic regulation between normal and tumor cells is different.[1] For example, previous study reports that cancer cells utilize glucose at higher rates than normal tissue. Furthermore, tumor cells use aerobic glycolysis with reduced mitochondrial oxidative phosphorylation for glucose metabolism and ultimately led to tumorigenesis.[2] While pyruvate kinase M2 (PKM2) regulates the rate-limiting final step of glycolysis.[3] Due to its fundamental function in tumor metabolism regulation, PKM2 has been proposed as antitumor drug target.[4]

The crystal structure of PKM2 was released in 2013 (pdb code: 4B2D).[5] The structure (Figure 1) includes four domains (A, B, C, N-terminus domains) and three binding sites of two allosteric sites for fructose-1,6-bisphosphate (FBP) and serine and one substrate site. It lays down the foundation for deciphering the molecular mechanisms of glycolysis, prompting many further questions, for example, 1) what is the relationship between these two allosteric effectors? 2) does there exist a synergistic allosteric mechanism? 3) how does the information transfer from the allosteric sites to the substrate site? and 4) what are the allosteric pathways in PKM2?

To answer these questions, dynamical correlation networks, which were previously used to illustrate the allosteric phenomenon of aminoacyl-tRNA synthetase,[6] were constructed based on all-atom molecular dynamics (MD) simulations of the wild type and mutant PKM2. From the comparisons of the networks between free and bound PKM2, the synergistic allosteric pathway was proposed for transferring the metabolism information from the FBP and serine allosteric sites to the substrate site. Multiple key residues were also identified to illustrate their roles in allosteric pathways.

Materials and Methods

Molecular dynamics simulation

The atomic coordinates of the PKM2 complex were extracted from PDB database (PDB code: 4B2D and 4FXF).[5, 7] S437Y and H464A are the mutants mentioned in the previous works to reveal the independent activation mechanism by FBP and serine, respectively.[5] R73A mutant also was used to reveal the regulation of activation by allosteric effectors. These mutant structures were constructed using SYBYL®-X 2.1.1.[8] All structural visualizations were conducted in PyMOL 1.7.[9]

All initial structures were first minimized in SYBYL®-X 2.1.1 to eliminate any possible overlaps or clashes. AMBER12 was used to perform efficient simulations with periodic boundary conditions.[10] Hydrogen atoms were added using the LEaP module of AMBER12. Counter-ions were used to maintain system neutrality. All systems were solvated in a truncated octahedron box of TIP3P waters with a buffer of 10 Å. The pairwise interactions (van der Waals and direct Coulomb) were computed with a cutoff distance of 8 Å. Particle Mesh Ewald (PME) was employed to treat long-range electrostatic interactions in AMBER12.[11] The improved ff99SBildn force field was used for the intramolecular interactions. The Langevin thermostat was used in the preparation runs with a friction constant of 1 ps^{-1} and the Berendson thermostat was used in the production runs.[9, 12] All MD simulations were accelerated with the CUDA version of PMEMD in GPU cores of NVIDIA® Tesla K20.

To relieve any further structural clash in the solvated systems, initial minimization with macromolecule frozen was performed using 500-step steepest descent minimization and 2000-step conjugate gradient minimization. Next the whole system was followed by 1000-step steepest descent minimization and 19000-step conjugate gradient minimization. After minimization, a 400-ps' heating up and a 200-ps' equilibration in the NVT ensemble at 310K were performed before MD simulation was conducted in the NPT ensemble at 310K.

To compare the difference among the chosen PKM2 systems, seven systems including four wild types and three mutants were simulated and detailed simulation conditions are listed in Table 1. 1.9 μs trajectories in all were collected at 310K.

Data analysis

Interaction assignment was handled with in-house software.[13, 14] The residues and substrate or effectors are in hydrophobic interaction when mass centers of their side chains and ligands are closer than 6.5 Å for the complex. A previous study has shown that charge-to-

charge interactions up to 11 Å were found to contribute to protein/protein binding free energies.[15] Thus, electrostatic (i.e. charge-charge) interactions are assigned when the distances between the mass centers of charge residues are less than 11 Å. Hydrogen bond is defined that the distance between the donor and acceptor is less than 3.5 Å and the bond angle is larger than 120 degree.

The landscape of distance difference was mapped by calculating normalized probability from a histogram analysis, and plotted with Origin 8.5. For each simulation, sampling was conducted every 10 ps. Radius of gyration (Rg) and root mean standard deviation (RMSD) were both separated into 8 bins. The energy landscape was plotted among these 64 (8×8) bins. Average structures were extracted from the structure ensembles of the lowest energy.[15-18]

MM/PBSA free energy calculation

Free-energy calculation together with MD simulations can provide quantitative predictions of PKM2–ligand binding energies. The free energy of binding (ΔG_{bind}) is estimated by Eq. 1.

$$\Delta G_{bind} = G_{R+L} - (G_R + G_L) \quad (1)$$

where G_{R+L}, G_R, and G_L is the free energies of the PKM2 complex, free PKM2, and the allosteric effectors or substrate, respectively. In the MM/PBSA approach,[16, 19-21] each free energy term in Eq. 1 is calculated as Eq. 2.

$$G = E_{bond} + E_{vdw} + E_{elec} + G_{PB} + G_{SA} - TS_S \quad (2)$$

where E_{bond} is the bond energy including the bond, angle and dihedral energies; E_{vdw} is the van der Waals energy contribution; E_{elec} is the electrostatic energy; G_{PB} and G_{SA} are the solvation energy corresponding to polar and non-polar contributions; T is the absolute temperature and S_S is the solute entropy. The PBSA model in MMPBSA was used to calculate the binding free energies.[16, 19-21] Only the last 50ns of MD trajectories from the equilibration period was employed to handle the binding free energy.

Correlation and Network Analyses

Every amino acid or ligand was defined as one node for dynamics network. The fluctuation correlation between any pair of nodes *i* and *j* was calculated with Equ. 3.

$$C_{ij} = \frac{\langle \Delta \vec{r_i}(t) \cdot \Delta \vec{r_j}(t) \rangle}{\sqrt{\left(\langle \Delta \vec{r_i}(t) \rangle^2 \langle \Delta \vec{r_j}(t) \rangle^2 \right)}} \quad (3)$$

where $\Delta \vec{r_i}(t) = \vec{r_i}(t) - \langle \vec{r_i}(t) \rangle$, $\vec{r_i}(t)$ is the position of node *i* at time *t*, and $\langle \cdot \rangle$ represents a time averaging. These elements were conveniently organized as a covariance

matrix for simulated system. In the current study, the covariance matrix for each system was constructed using snapshots (every 2 ps) in the last 50 ns of all simulated trajectories. Besides nodes, “edge” that transfers allosteric information from one node to another is defined between any two nodes without covalent bond and the distance between two heavy atoms from two nodes are closer than 4.5 Å over 75% sampling time. The strength of the edge between nodes i and j is defined as the absolute value of the inter-node correlation (C_{ij}). The number of connected edges at each node is defined as the degree of the node. Correlation-weighted degree, which is the summation of strengths of all edges connected to a given node, indicates the importance of the node. After the network construction, Cytoscape3.1.1[22] was used to calculated the network topological parameters. The shortest path between any two nodes in the network was identified with the Floyd-Warshall algorithm. Girvan-Newman algorithm was utilized to build the community network.[6, 23, 24]

Results

Stability of PKM2 in free and complex states

Cα RMSD relative to the initial structure shows that 150 ns simulations are sufficient for the equilibration of the wild types and mutant systems at 310K (supplementary Figure S1). Root mean squared fluctuations of Cα atom for four wild type systems are shown in Figure 2. To our surprise, Cα variation of the bound PKM2 is much higher than that of the free PKM2, especially for the residues of domain B. The observed flexibility difference might be induced by the allosteric effectors of FBP and serine. That is, domain B becomes obvious unstable upon FBP and serine binding. This phenomenon is also confirmed by the systems of FBP/PKM2 and Ser/PKM2.

In order to evaluate the conformational adjustment of PKM2, pairwise Cα distance difference between bound and free PKM2 was analyzed. Figure 3 illustrates the conformational adjustment of PKM2 upon binding FBP and serine. Blue regions represent negative differences, indicating more compact structure, while red regions indicate Cα atoms pushed further away (more extended structure). In this figure, red regions are located between residues 100 and 200, suggesting that domain B moves further away from domain C upon FBP and serine binding. Consistent observations are also found in the principal component analysis (PCA) as to be discussed below.

Distance different landscape indicates that domain B undergoes significant conformational changes. To quantitatively identify the conformational adjustment, PCA was carried out on the four wild type systems to study the motion mode. Overall the three most dominant components (named PC1, PC2, and PC3) represent over 67% of the overall fluctuations. In addition, B and C domains contribute most of the fluctuations. To clearly display the motion of B and C domains, structural projections along the first principal component (~40%) are shown in Figure 4. For the free PKM2, no significant conformational changes were observed. Upon binding allosteric effectors of FBP and serine, B and C domains of bound PKM2 are in the opening motion mode. This motion was induced by the binding of allosteric effectors. We can also find similar motion mode for B and C domains of FBP/PKM2 and Ser/PKM2.

To confirm the reliability and robustness of MD simulations, the binding free energies between allosteric effector (FBP or serine) and PKM2 for the wild type and mutants are calculated with MMPBSA[16, 19-21] and listed in Table 2. Although the binding free energies were over-estimated because of the limitations of the MMPBSA approach, it is still possible to extract interesting conclusions from the difference of free energy between mutant and wild type [25]. The MMPBSA analysis shows that the binding free energy of the wild type is always lower than that of mutant. For example, the binding free energy between FBP and PKM2 for the S437Y mutant is about 17.55 kcal/mol higher than that of bound PKM2. This is in qualitative agreement with experiment in that the S437Y mutant significantly decreases the binding affinity of FBP [26]. At the same time, the binding free energy between serine and PKM2 for the H464A mutant is 16.87 kcal/mol higher than that of the wild type. This is also consistent with experiment in that serine cannot directly bind PKM2 for the H464A mutant [5]. In summary, the MD simulation and binding free energy analysis are in good accord with previous experimental observations [5, 26].

Correlation Networks of Free and PKM2 Complex Are Different

In order to reveal the allosteric mechanism, the dynamic correlation network analysis was used to illustrate the residue fluctuation correlation. To construct the correlation network, the covariance matrices were first calculated. Then fluctuation correlation networks were built. The topology parameters of network for four wild systems are listed in Table 3.

The values of topology parameters for network of the bound PKM2 are the highest among these four systems. This suggests that the characters of network for the bound PKM2 are significant different from those of other systems. The correlation networks for the bound and the free PKM2 are shown in Figure 5. It shows that the number of nodes with weighted degree higher than 10 (more than 10 edges) is 10 in the bound network and more than that of the free network (6). [Does the previous sentence define the hub nodes?] The important hub nodes might play key roles in network model, such as R73, H84, L61, M64, T363, K270, I283, I181, V197, and FBP, with higher degree in the bound PKM2 network. The correlation networks for FBP/PKM2 and Ser/PKM2 are shown in supplementary Figure S2. The number of nodes with weighted degree higher than 10 for FBP/PKM2 or Ser/PKM2 is also more than that for the free PKM2. This suggests that the allosteric effectors indeed increase the correlation of nodes for PKM2 complex.

In order to illustrate the differences of networks among the four systems, a Wilcoxon test was used to analyze the correlation-weighted degrees of any two networks (Table 4). The *P*-values among these four systems are less than 0.05, indicating that the networks among the four systems have significantly difference. This is consistent with the results of topology parameter for the network.

Information Transfer Pathways in the Networks

The analysis of correlation network shows that the networks are significantly different among the four simulated systems. To reveal the information transfer pathways, the Girvan-Newman algorithm was used to split these networks into communities. The community network analysis (Figure 6) shows that the community network of the free PKM2 has 14

communities including three isolated clusters (gray). The information difficultly transfers from domain B to domain C in the fragmented network. However the community network becomes more centralized upon binding to FBP and/or serine: there are only 10 communities with one isolated cluster for FBP/PKM2; 9 communities with one isolated cluster for Ser/PKM2; and only 8 communities without isolated cluster for the bound PKM2. This demonstrates that the effects of binding to both FBP and serine are needed for optimal integrity of the community in the complexes. The relevant residues belonging to each community for free and bound PKM2 are listed in Tables S1-S2. Isolated cluster of community 2 includes A215 and D217 that located at the loop between domains C and A, and isolated cluster 4 includes P517 which is near the binding pocket of FBP. That is, the information could not freely transfer from FBP allosteric pocket to substrate site for free PKM2. However, for the connected community network of the bound PKM2, the information flow can freely transfer from FBP and serine allosteric sites to the substrate site. Relevant residues associated with each community for FBP/PKM2 and Ser/PKM2 are listed in Tables S3-S4. There are some isolated residues of A215 or P517 [incomplete logic flow]. Of course the information flow can also transfer for FBP to substrate for FBP/PKM2 or from serine to substrate for Ser/PKM2. However, the efficiency of information transfer would be reduced in the more fragmented community networks with isolated cluster than bound PKM2. This will be confirmed by the allosteric pathway analysis below.

Moreover, structural analysis indicates that there are eleven hydrogen bonds and five electrostatic interactions between FBP and PKM2, and three hydrogen bonds and five electrostatic interactions between serine and PKM2 with population higher than 40% (supplementary Figure S3) in the bound PKM2. Thus two allosteric effectors introduce strong interactions with PKM2. Furthermore, the binding free energy between the substrate and PKM2 for bound PKM2 is significantly lower than that for FBP/PKM2 or Ser/PKM2 (listed in Table 5). Their binding effects for FBP and serine in the community network lead us to propose the hypothesis of “synergistic allosteric mechanism” to explain the regulation mode for PKM2.

Modifications Used to Perturb the Community Network

In order to validate the above hypothesis, modifications to weaken the interactions between FBP or serine and PKM2 for bound PKM2 were used to study the effects on the community networks. These modifications were realized by just deleting the edges between FBP or serine and PKM2 nodes in the network. The community networks of weakened systems are shown in Figure 7. [In the following you want to lead readers first that these weakening operations lead to more fragmented networks, therefore less efficient info flow. And what quantitative measure is used to show this (number of communities? But this is not always true.)] For the weakened FBP, the number of community increases from 8 to 9 including an isolated community. The connections between domain B and domain A increase two from one. For the weakened serine, the number of communities decreases from 11 from 8. Furthermore, domains B and C are split into more communities than that of bound PKM2. In both weakened community networks, there are 11 communities and more than those of the bound PKM2 [The two highlighted sentences are conflicting.]. At the same time, there are two isolated communities in weakening system.

In addition, the relevant residues belonging to each community for FBP and/or serine modifications are listed in Tables S5-S6. These residues in community are significantly different among these systems [You need to say why they can reduce flow efficiency]. In summary these modifications lead to significant repartition of the community networks [You have to say why this repartition matters.]. This finding confirms that the interactions between FBP/serine and PKM2 indeed influence the community network and further support our hypothesis of synergistic allosteric mechanism.

Validation of Synergistic Allosteric Mechanism by Mutation

In order to evaluate the independent activation of PKM2 by either FBP or serine, previous work reports two mutants of S437Y and H464A [5], demonstrating that the H464A mutant is activated by FBP but the binding to serine is abolished [5]. Conversely, the S437Y mutant is activated by serine but the binding to FBP is abolished [26]. Both mutants decrease ~ 9-19 fold activation in the bound PKM2. To further evaluate the hypothesis of "synergistic allosteric mechanism", the networks of these mutants are constructed and shown in supplementary Figure S4, indicating that their networks are different from that of wild type for bound PKM2.

The community networks of the two mutants are shown in Figure 8. There is one isolated community and the number of community increases to 12 for the H464A mutant. For the S437Y mutant, even the number of community has not significant change, the residues belong to each community are different from those of wild type (listed in Tables S8-S9). [There is a logical gap here from what you see and what you conclude next.] Even if the information can transfer from the FBP or serine allosteric site to the substrate site, the efficiency is reduced due to the fragmentation of the community networks, leading to reduced allosteric effect.

FBP and Serine Allosteric Pathways

The network and community analyses of the wild type and mutants confirm that the FBP and serine binding induces synergistic allostery of PKM2. Next, it is natural to identify the synergistic allosteric pathway based on the shortest path analysis which was used to identify the allosteric pathway between the allosteric site and the active site.[27] Two pathways were identified in the bound PKM2: FBP, K433, T459, R461, A109, V71, R73, MG2, OXL (oxalic acid) and SER, I47, C49, R73, MG2, OXL (Figure 9A). However, we could not find a similar pathway in the free PKM2. This indicates that K433, T459, R461, A109, V71, R73, I47, and C49 are key nodes for information transfer in the bound PKM2. Two communication pathways along with strong correlation residues between the allosteric site and the substrate site are shown in supplementary Figure S5. These strong correlation residues may play certain roles in allosteric effectors. Note also that the information intensity of the shortest pathway for the bound PKM2 community network (10.30) is also higher than the sum of similar pathways in FBP/PKM2 (4.92) and Ser/PKM2 (4.07). This indicates that the efficiency of information transfer is 47.77% for FBP/PKM2 and 39.51% for Ser/PKM2 if the bound PKM2 efficiency is 100%. This further supports the hypothesis of synergistic allosteric mechanism.

Hypothetical network alteration was used to validate the two allosteric pathways. Worth noting is that R73 is at the junction of the two proposed pathways and is thus crucial for the information flow. In order to further confirm the key function of R73, the R73A mutant was simulated for 150 ns. The binding free energy between substrate and PKM2 was about −44.99 ± 5.46 kcal/mol and much higher than that of wild type. The community of R73A is shown in Figure 9B. Four isolated clusters were found. The number of community increases from 8 to 12. Therefore, the efficiency of information flow is significantly reduced due to the fragmentation of the network. This suggests that the proposed allostery pathways, at least R73 before the junction, play key roles in the synergistic allostery.

Discussion

Conformation Adjustment Corresponding to Synergistic Allostery

In order to illustrate the relationship between synergistic allostery and conformation adjustment, the average RMSDs between free and bound PKM2 among 3 trajectories vs. the distances from the allosteric site (FBP or serine) are shown in Figure 10. The RMSD first fluctuates, and then reaches a plateau for the FBP site. This suggests that the area of conformational change did not just focus on the FBP binding site, but also extended to the substrate site. The conformation distributions between free and bound PKM2 were evaluated with two sample Kolmogorov–Smirnov (KS) test.[28] In order to investigate the statistical significance for the conformational deviations, the KS *P* value test was analyzed. Note that the KS test, as a nonparametric test, is a good choice for this study because the conformation distributions do not fit well to any distribution used for parametric tests. As shown in Figure 10B, the conformational differences are statistically significant up to 60Å away from the FBP binding site, with the median *P* values typically less than 0.05. This suggests that the allosteric effect can be far away from the allosteric site of FBP.

At the serine binding site, the RMSD gradually increases and then reaches a plateau (Figure 10C). This suggests that the area of conformational change is far away from the binding site of serine. The KS test also suggests that the conformational differences are statistically significant up to 50Å away from the serine allosteric site. In summary, both FBP and serine allosteric effectors significantly induce long-range conformational adjustments in the MD simulations.

Conformation Adjustments *via* Community Networks

In order to further link the conformational adjustments and the community network for bound PKM2, the dynamical cross-correlation map (DCCM) was used in this study[29] and the DCCMs of free and bound PKM2 are shown in Figure 11. The figure suggests that the correlations among residues are small and consistent with the slight conformational change for free PKM2. It is interesting to see that residues 100-200 of domain B are strongly correlated with residues 400-500 of domain C and anti-correlated with residues 20-100 of N-terminus domain. Residues 200-400 of domain A are also strongly anti-correlated with residues 100-200 of domain B. Domain C has strongly correlation/anti-correlation with N-terminus, A and B domains. These results indicate that the conformational adjustments of bound PKM2 are through the interaction between different domains. Note also, the network

of bound PKM2 has more hub nodes than that of free PKM2. The similar results are also found that the residues among these domains have strong correlation and correlated with conformational change for FBP/PKM2 and Ser/PKM2 (shown in supplementary Figure S6).

Comparison with Previous Experiments

The previous work reports that *in vitro* activity of recombinant human PKM2 is about 35-fold activation in the presence of FBP or serine, while the activity of the H464A mutant is about 26-fold activation in the presence of FBP and the S437Y mutant is about 6-fold activation in the presence of serine.[5] Although PKM2 can be independently activated by FBP or serine, these mutations destroy the allosteric pathway of FBP or serine and the activity of PKM2 will significantly decrease from 9 to 29-fold. This partially supports the synergistic allosteric mechanism of PKM2 upon FBP and serine binding.

The structural analysis has shown that Arg43, Asn44, and Arg106 are the critical residues in stabilizing the complex.[5] Two stable electrostatic interactions were found for Arg43/serine and Arg106/serine in our room temperature simulation. Furthermore, a stable hydrogen bond was formed between Asn44 and serine. These results are in good agreement with the structure analysis that Arg43, Asn44, and Arg106 form important interactions with serine. The literature also illustrates that Thr432, Lys433, Ser434, Ser437, Trp482, Arg489, Glu514, Gly518, Ser519, Gly 520, and Phe521 form important interactions for the wild type between FBP and PKM2.[30] Eleven stable hydrogen bonds and five electrostatic interactions were found in simulation with population higher than 40%, such as Ser519/FBP, Thr432/FBP, Ser434/FBP, Lys433/FBP, Arg489/FBP, between FBP and PKM2. These results are also in agreement with the structural analysis.[5]

In order to confirm the synergistic allostery mechanism, the driver/anchor atom analysis was also used in this study. Nussinov *et al* reports that driver and anchor atoms exhibit specific interactions with the host protein, with the driver atoms mainly responsible for the allosteric efficacy and the anchor atoms for the binding affinity.[31] In order to identify the possible driver and anchor atoms in bound PKM2, the global backbone displacement (GBD) of corresponding atom pairs [31] were used to assign the possible driver and anchor atoms. The results are shown in Figure 12. These functional atoms might play key roles in the allosteric activation in PKM2. In summary, the driver/anchor analysis was in agreement with Kolmogorov–Smirnov (KS) *P* value test that the allosteric effect can be far away from the allosteric sites.

Conclusion

Residue/residue fluctuation correlation network was used to reveal the allosteric mechanism of PKM2 upon binding to allosteric effectors of FBP and serine. The results suggest that the dynamics correlation network of bound PKM2 has more hub nodes than that of the free state. The community network of the bound PKM2 is clustered into an intact community without isolated cluster. However, there are three isolated clusters for free PKM2. The information flow can freely transfer from the FBP and serine allosteric sites to the substrate site for bound PKM2. The efficiency of information transfer for bound PKM2 is higher than that of FBP/PKM2 or serine/PKM2. The binding free energy between the substrate and

PKM2 for the bound PKM2 is significantly lower than that of one allosteric effector system. Therefore, a hypothesis of “synergistic allosteric mechanism” is used to explain the PKM2 glycolysis and FBP/serine binding. These observations were further confirmed by community analysis based on the Girvan-Newman algorithm for two mutants and network-weakened systems. Finally, two possible allosteric pathways are also identified based on the analysis of the network for bound PKM2 and confirmed by network perturbation. Interestingly, no similar pathways could be found in other systems.

Supplementary Material

Refer to Web version on PubMed Central for supplementary material.

Acknowledgements

This work was supported by Center for HPC at Shanghai Jiao Tong University, the Ministry of Science and Technology of China (2012CB721003), the National High-tech R&D Program of China (863 Program) (2014AA021502), the National Natural Science Foundation of China (J1210047 and 31271403), Medical Engineering Cross Fund of Shanghai Jiaotong University (YG2013MS68, YG2014MS47, and YG2015MS56), and National Institutes of Health/NIGMS (GM093040 & GM079383).

References

1. Christofk HR, Vander Heiden MG, Wu N, Asara JM, Cantley LC. Pyruvate kinase M2 is a phosphotyrosine-binding protein. Nature. 2008; 452:181–186. [PubMed: 18337815]
2. Warburg O. On the origin of cancer cells. Science. 1956; 123:309–314. [PubMed: 13298683]
3. Majumder PK, Febbo PG, Bikoff R, Berger R, Xue Q, McMahon LM, Manola J, Brugarolas J, McDonnell TJ, Golub TR, Loda M, Lane HA, Sellers WR. mTOR inhibition reverses Akt-dependent prostate intraepithelial neoplasia through regulation of apoptotic and HIF-1-dependent pathways. Nat. Med. 2004; 10:594–601. [PubMed: 15156201]
4. Vander Heiden MG. Targeting cancer metabolism: a therapeutic window opens. Nat. Rev. Drug Discov. 2011; 10:671–684. [PubMed: 21878982]
5. Chaneton B, Hillmann P, Zheng L, Martin AC, Maddocks OD, Chokkathukalam A, Coyle JE, Jankevics A, Holding FP, Vousden KH, Frezza C, O'Reilly M, Gottlieb E. Serine is a natural ligand and allosteric activator of pyruvate kinase M2. Nature. 2012; 491:458–462. [PubMed: 23064226]
6. Sethi A, Eargle J, Black AA, Luthey-Schulten Z. Dynamical networks in tRNA:protein complexes. Proc. Natl. Acad. Sci. USA. 2009; 106:6620–6625. [PubMed: 19351898]
7. Morgan HP, O'Reilly FJ, Wear MA, O'Neill JR, Fothergill-Gilmore LA, Hupp T, Walkinshaw MD. M2 pyruvate kinase provides a mechanism for nutrient sensing and regulation of cell proliferation. Proc. Natl. Acad. Sci. USA. 2013; 110:5881–5886. [PubMed: 23530218]
8. SYBYL-X Suite, version 2.1.1. Certara: Princeton, NJ: 2012.
9. Jawallapersand P, Mashele SS, Kovacic L, Stojan J, Komel R, Pakala SB, Krasevec N, Syed K. Cytochrome P450 Monooxygenase CYP53 Family in Fungi: Comparative Structural and Evolutionary Analysis and Its Role as a Common Alternative Anti-Fungal Drug Target. PloS one. 2014; 9:e107209. [PubMed: 25222113]
10. Case, DA.; Darden, TA.; Cheatham, ITE.; Simmerling, CL.; Wang, J.; Duke, RE.; Luo, R.; Walker, RC.; Zhang, W.; Merz, KM.; Roberts, B.; Hayik, S.; Roitberg, A.; Seabra, G.; Swails, J.; Götz, AW.; Kolossváry, I.; Wong, KF.; Paesani, F.; Vanicek, J.; Wolf, RM.; Liu, J.; Wu, X.; Brozell, SR.; Steinbrecher, T.; Gohlke, H.; Cai, Q.; Ye, X.; Wang, J.; Hsieh, MJ.; Cui, G.; Roe, DR.; Mathews, DH.; Seetin, MG.; Salomon-Ferrer, R.; Sagui, C.; Babin, V.; Luchko, T.; Gusarov, S.; Kovalenko, A.; Kollman, PA. AMBER 12. University of California; San Francisco: 2012.
11. Darden T, York D, Pedersen L. Particle mesh Ewald: An N· log (N) method for Ewald sums in large systems. J. Chem. Phys. 1993; 98:10089–10092.

12. Baron R, Vellore NA. LSD1/CoREST is an allosteric nanoscale clamp regulated by H3-histone-tail molecular recognition. Proc. Natl. Acad. Sci. USA. 2012; 109:12509–12514. [PubMed: 22802671]
13. Wang W, Ye W, Jiang C, Luo R, Chen HF. New force field on modeling intrinsically disordered proteins. Chem. Biol. Drug Des. 2014; 84:253–269. [PubMed: 24589355]
14. Huang Z, Zhu L, Cao Y, Wu G, Liu X, Chen Y, Wang Q, Shi T, Zhao Y, Wang Y, Li W, Li Y, Chen H, Chen G, Zhang J. ASD: a comprehensive database of allosteric proteins and modulators. Nucleic. Acids Res. 2011; 39:D663–669. [PubMed: 21051350]
15. Qin F, Chen Y, Wu M, Li Y, Zhang J, Chen HF. Induced fit or conformational selection for RNA/U1A folding. RNA. 2010; 16:1053–1061. [PubMed: 20354153]
16. Miller BR III, McGee TD Jr, Swails JM, Homeyer N, Gohlke H, Roitberg AE. MMPBSA. py: An efficient program for end-state free energy calculations. J. Chem. Theory Comput. 2012; 8:3314–3321. [PubMed: 26605738]
17. Chen HF. Mechanism of coupled folding and binding in the siRNA-PAZ complex. J. Chem. Theory Comput. 2008; 4:1360–1368. [PubMed: 26631711]
18. Chen HF, Luo R. Binding induced folding in p53-MDM2 complex. J. Am. Chem. Soc. 2007; 129:2930–2937. [PubMed: 17302414]
19. Wang J, Cai Q, Xiang Y, Luo R. Reducing Grid Dependence in Finite-Difference Poisson-Boltzmann Calculations. J. Chem. Theory Comput. 2012; 8:2741–2751. [PubMed: 23185142]
20. Wang J, Luo R. Assessment of Linear Finite-Difference Poisson-Boltzmann Solvers. J. Comput. Chem. 2010; 31:1689–1698. [PubMed: 20063271]
21. Cai Q, Hsieh M-J, Wang J, Luo R. Performance of Nonlinear Finite-Difference Poisson-Boltzmann Solvers. J. Chem. Theory Comput. 2010; 6:203–211. [PubMed: 24723843]
22. Shannon P, Markiel A, Ozier O, Baliga NS, Wang JT, Ramage D, Amin N, Schwikowski B, Ideker T. Cytoscape: a software environment for integrated models of biomolecular interaction networks. Genome Res. 2003; 13:2498–2504. [PubMed: 14597658]
23. Stone J, Developers NT, Eargle J, Sethi A, Li L, Luthey-Schulten Z. Dynamical Network Analysis. 2012
24. Girvan M, Newman ME. Community structure in social and biological networks. Proc. Natl. Acad. Sci. USA. 2002; 99:7821–7826. [PubMed: 12060727]
25. Furini S, Barbini P, Domene C. DNA-recognition process described by MD simulations of the lactose repressor protein on a specific and a non-specific DNA sequence. Nucleic. Acids Res. 2013; 41:3963–3972. [PubMed: 23430151]
26. Allali-Hassani A, Wasney GA, Chau I, Hong BS, Senisterra G, Loppnau P, Shi Z, Moult J, Edwards AM, Arrowsmith CH, Park HW, Schapira M, Vedadi M. A survey of proteins encoded by non-synonymous single nucleotide polymorphisms reveals a significant fraction with altered stability and activity. Biochem. J. 2009; 424:15–26. [PubMed: 19702579]
27. Rodriguez-Puente R, Lazo-Cortes MS. Algorithm for shortest path search in Geographic Information Systems by using reduced graphs. SpringerPlus. 2013; 2:291. [PubMed: 24010024]
28. Wlodarski T, Zagrovic B. Conformational selection and induced fit mechanism underlie specificity in noncovalent interactions with ubiquitin. Proc. Natl. Acad. Sci. USA. 2009; 106:19346–19351. [PubMed: 19887638]
29. Ghosh A, Vishveshwara S. A study of communication pathways in methionyl- tRNA synthetase by molecular dynamics simulations and structure network analysis. Proc. Natl. Acad. Sci. USA. 2007; 104:15711–15716. [PubMed: 17898174]
30. Dombrauckas JD, Santarsiero BD, Mesecar AD. Structural basis for tumor pyruvate kinase M2 allosteric regulation and catalysis. Biochemistry. 2005; 44:9417–9429. [PubMed: 15996096]
31. Nussinov R, Tsai CJ. Unraveling structural mechanisms of allosteric drug action. Trends Pharmacol. Sci. 2014; 35:256–264. [PubMed: 24742712]

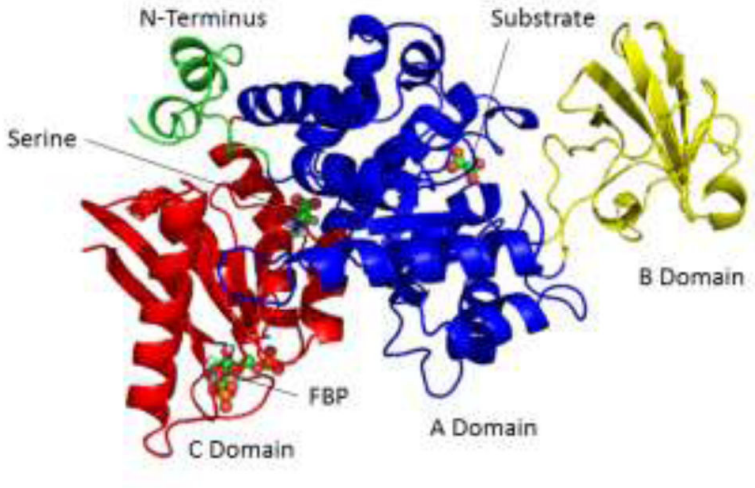

Figure 1.

Ribbon representation of the crystal structure for bound PKM2. N-terminus (green), A Domain (blue), B Domain (yellow), C Domain (red), FBP, serine, and substrate are labeled, respectively.

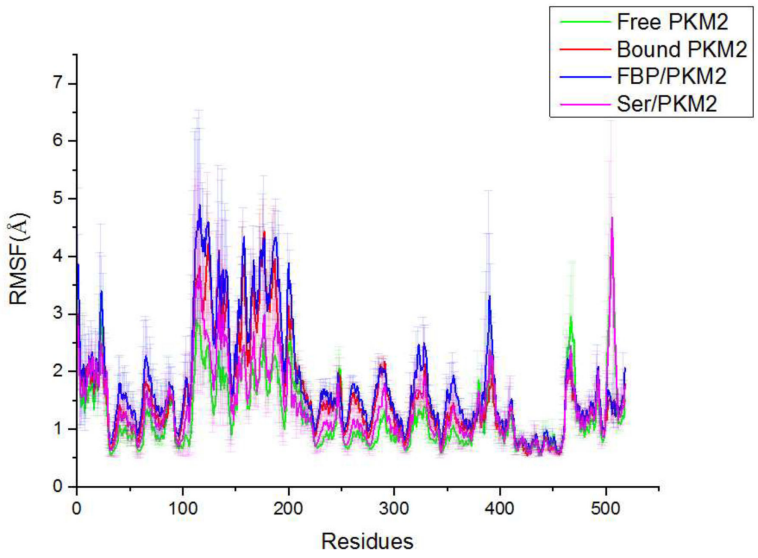

Figure 2.
Average fluctuations of Cα atoms for four systems.

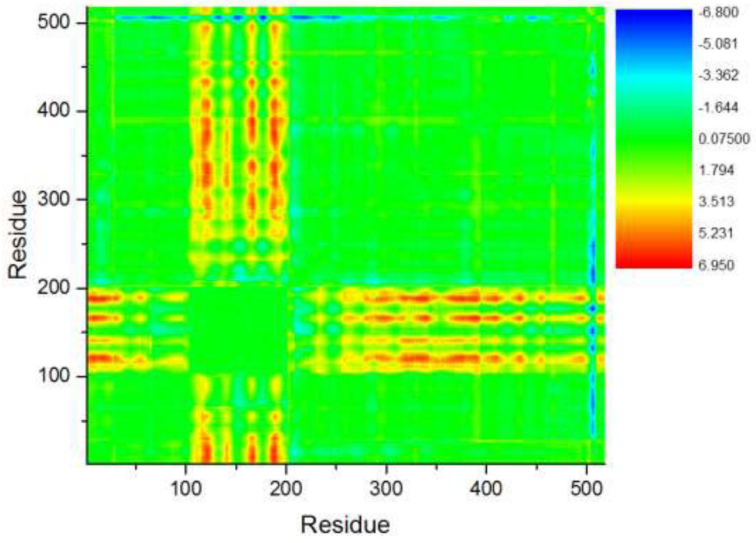

Figure 3.

Pairwise Cα distance difference between bound PKM2 and free PKM2. Red regions mean the average distance between related atoms pair (Cα-Cα) in bound structure is larger than in free structure (extension upon binding); correspondingly, blue regions mean compaction upon binding.

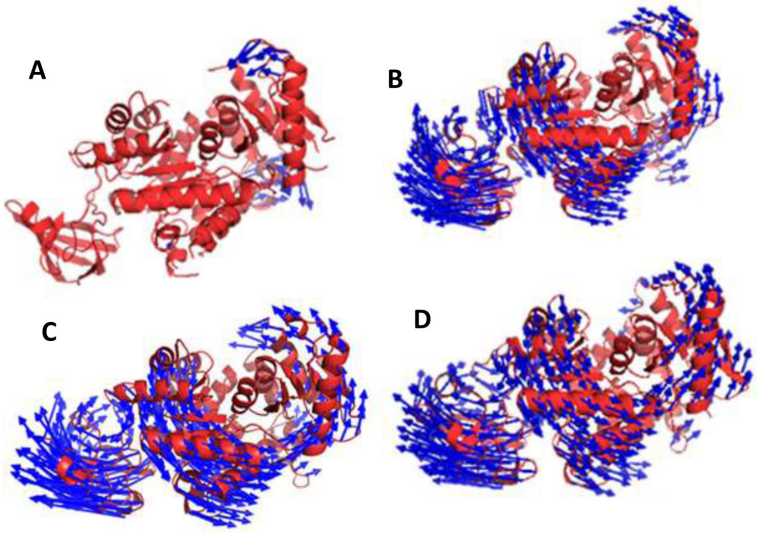

Figure 4.
Motion modes from PCA analysis. A: Free PKM2. B: FBP/PKM2. C: Ser/PKM2. D: Bound PKM2.

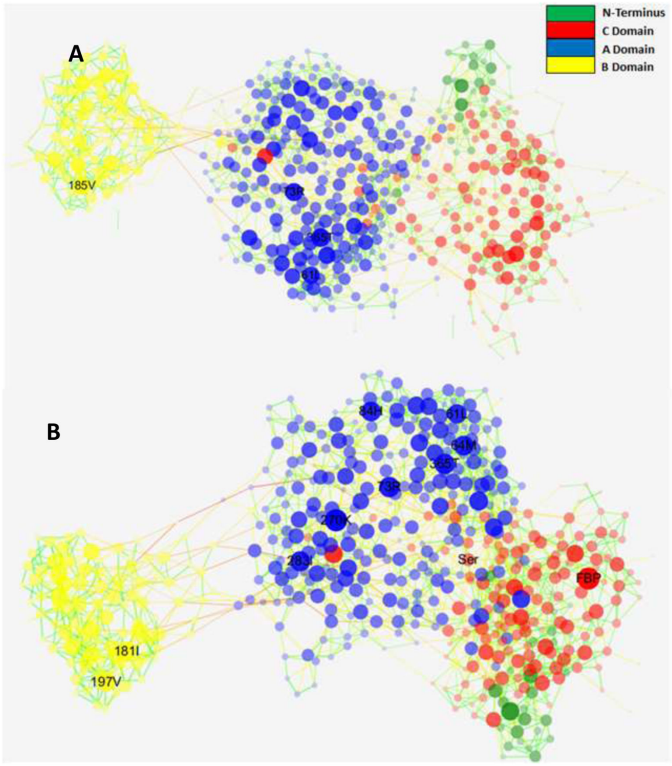

Figure 5.

Correlation networks for free and bound PKM2. The size of node is drawn based on the value of correlation-weighted degree and the color of node according to its structural domain. Node with correlation-weighted degree higher than 10.0 is labelled with the name of residue. Edges are colored with their betweennesses, thin green lines for lower betweenness and thick red lines for higher betweenness. A: free PKM2. B: bound PKM2.

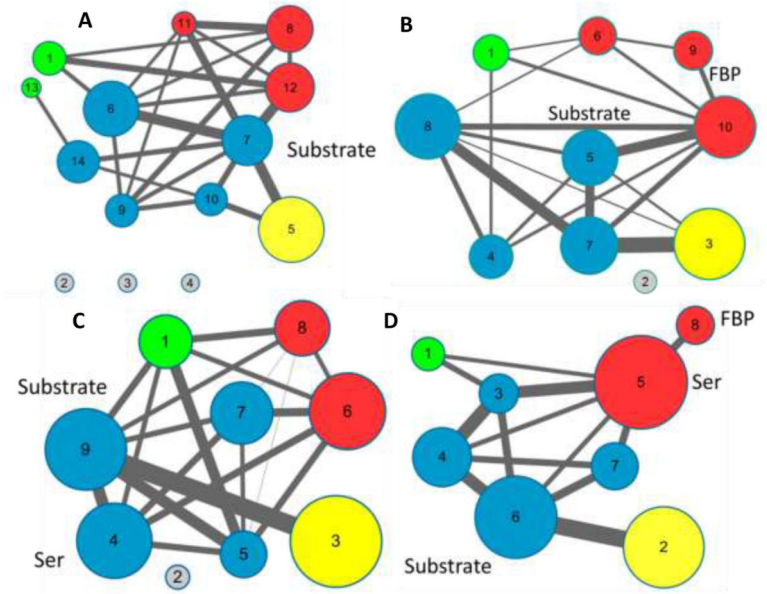

Figure 6.

Community networks for free and the complex PKM2. A: free PKM2. B: FBP/PKM2. C: Ser/PKM2. D: bound PKM2. Communities were split using the Girvan-Newman algorithm based on the edges and correlations between nodes in the dynamic correlation networks. Different colors represent different domains. Blue represents domain A, yellow for domain B, red for domain C, green for N-terminus, gray for isolated cluster without connection with other residues.

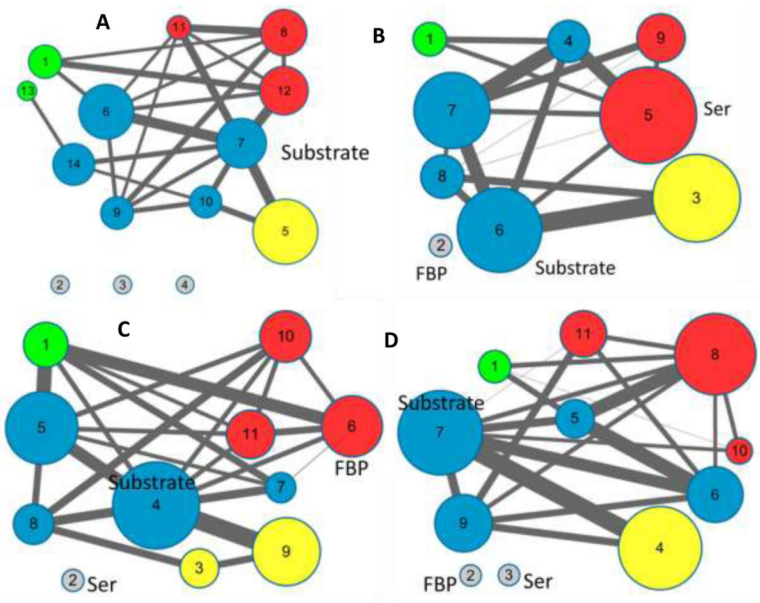

Figure 7.
Communities of weakened systems for bound PKM2. A: Free PKM2 as control. B: FBP Weakened. C: Serine Weakened. D: Both FBP and serine weakened.

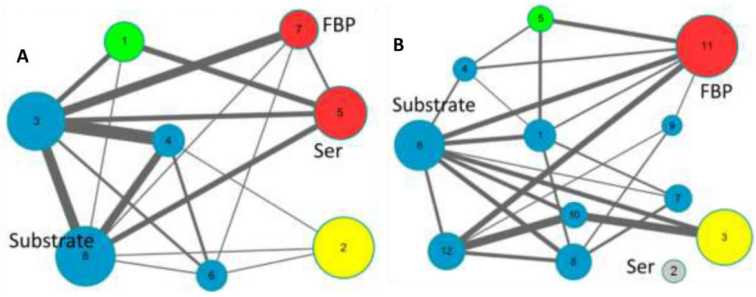

Figure 8.
Mutant community networks for bound PKM2. A: S437Y mutant. B: H464A mutant.

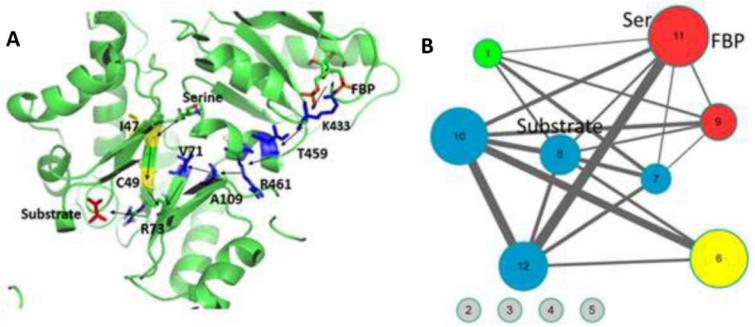

Figure 9.

FBP and serine allosteric pathways in bound PKM2. A: Shortest pathway from FBP and serine binding sites to substrate site. B: Community network of R73A mutant.

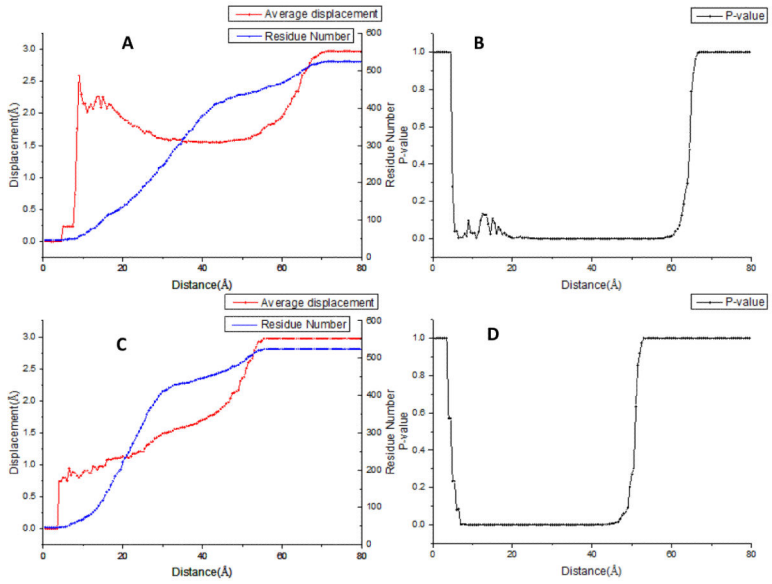

Figure 10.

Cα atomic RMSD (red lines) and number of included atoms (blue lines) vs. distance from FBP or serine allosteric site in bound PKM2. The data were averaged over three sets of simulated Bound and free PKM2 trajectories. Significance of local structural changes was elaborated by the Komogorov–Smirnov test, shown with median of P values. (A) RMSD vs distance from the FBP binding site; (B) KS test for the FBP binding site; (C) RMSD vs distance from the serine binding site; (D) KS test for the serine binding site.

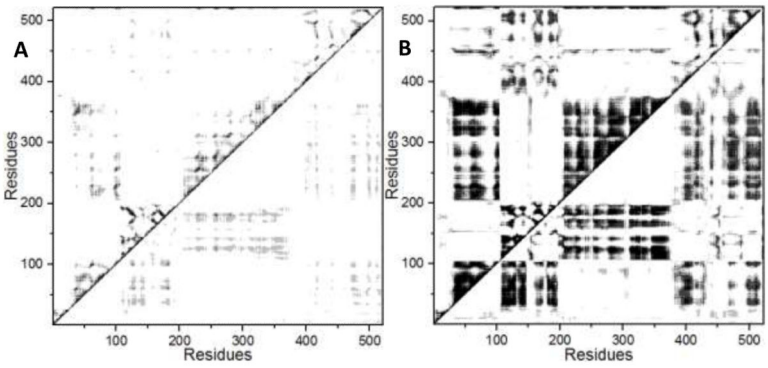

Figure 11.

Dynamical cross-correlation map for free and bound PKM2. A: free PKM2. B: bound PKM2. The strong (C_{ij}=±0.7-1.0), moderate (C_{ij}=±0.5-0.7), and weak (C_{ij}=±0.3-0.5) ones are colored with black, black gray, and slight gray, respectively. The lower and upper triangles correspond to negative and positive correlations, respectively.

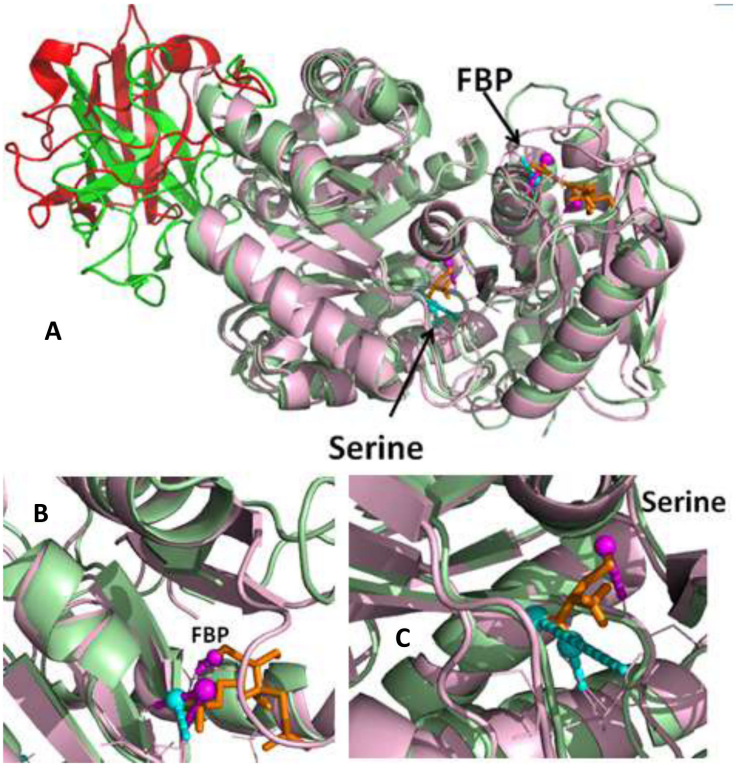

Figure 12.

Identification of driver and anchor atoms in bound PKM2. A: Global view. B: Zoomed-in at the FBP-binding region. C: Zoomed-in at the serine-binding region. The driver atom is labeled as a cyan sphere and the anchor atom is labeled as a magenta sphere. The residue that interacts with the driver atoms of FBP is S434. Residues that interact with anchor atoms are L431 and T432. The residues that interact with the driver atoms of serine are R43 and R106. Residue that interacts with anchor atoms is N44. PKM2 is represented as ribbon. FBP and serine are depicted as stick. The dark color of the ribbons indicates regions with large conformational changes, where the global backbone displacement (GBD) of corresponding pairs is greater than a preset distance (0.8Å). The local structural environment (LSE) is 0.9Å, the driver atom is in cyan sphere and the critical anchor atom in magenta sphere, with the corresponding dash line representing the interactions of driver and anchor atoms with the residues around. The driver and anchor atoms were identified with given operational structural criteria with a GBD of 0.8 Å and LSE of 0.9 Å.

Table 1

Simulation conditions for seven studied systems.

System	Composition	Temp (K)	Time (ns)	No. Traj.	Ions
Free PKM2	PKM2		100	3	2 Mg^{2+}, 1 K^{+}, 1Cl−
Ser/PKM2	Ser/PKM2	310	100	3	2 Mg^{2+}, 1 K^{+}, 1Cl−
Bound PKM2	FBP/Ser/PKM2		100	3	2 Mg^{2+}, 4 K^{+}
FBP/PKM2	FBP/PKM2		150	3	2 Mg^{2+}, 4 K^{+}
S437Y	FBP/Ser/PKM2		150	1	2 Mg^{2+}, 4 K^{+}
H464A	FBP/Ser/PKM2		150	1	2 Mg^{2+}, 4 K^{+}
R73A	FBP/Ser/PKM2		150	1	2 Mg^{2+}, 5 K^{+}

Table 2

Binding free energies (kcal/mol) between allosteric effectors and PKM2.

System	ΔG between FBP and PKM2	System	ΔG between serine and PKM2
Bound PKM2	−104.3 ± 14.8	Bound PKM2	−19.3 ± 4.7
S437Y	−86.75 ± 7.61	H464A	−2.43 ± 3.18

Table 3

Network parameters for free and bound systems.

Parameters	Free PKM2	Ser/PKM2	FBP/PKM2	Bound PKM2
Number of edges	1873	1913	1891	1935
Clustering coefficient	0.253	0.260	0.263	0.267
Network centralization	0.013	0.013	0.017	0.02
Avg number of neighbors	7.20	7.326	7.259	7.396
Number of nodes	520	522	521	523

Table 4

P-values of Wilcoxon test among four PKM2 systems.

System	Bound PKM2	FBP/PKM2	Ser/PKM2
Free PKM2	0.0199	3.01e-27	3.05e-59
Bound PKM2	-	7.00e-22	1.20e-31
FBP/PKM2	-	-	1.25e-5

Table 5

Binding free energies between substrate and PKM2.

System	Binding free energy (kcal/mol)					Average
	50-60ns	60-70ns	70-80ns	80-90ns	90-100ns	
Bound PKM2	−59.98 ± 5.95	−59.95 ± 5.78	−59.38 ± 5.77	−58.86 ± 6.10	−59.11 ± 6.16	−59.46±0.50
Free PKM2	−30.82 ± 5.33	−30.25 ± 4.97	−31.71 ± 5.80	−40.16 ± 5.60	−45.65 ± 4.80	−35.72±6.86
Ser/PKM2	−53.40 ± 5.67	−50.45 ± 4.74	−46.59 ± 4.98	−47.14 ± 5.08	−45.91 ± 5.03	−48.70±3.16
FBP/PKM2	100-110ns	110-120ns	120-130ns	130-140ns	140-150ns	−54.56±2.76
	−53.91 ± 4.42	−57.32 ± 5.02	−56.71 ± 5.37	−54.50 ± 5.36	−50.34 ± 4.98	